

## A COMPARISON OF DIFFERENT OPTICAL TECHNIQUES FOR COPPER CANISTER AUTHENTICATION AND APPLIED FORENSICS

Stefanie Neutzner<sup>1</sup>, Aurora Fassi<sup>1</sup>, Gunnar Boström<sup>1</sup>

<sup>1</sup>European Commission, Joint Research Centre (JRC), Ispra (VA), Italy

### ABSTRACT

One of the challenges of nuclear safeguards for spent fuel storage in long-term geological repositories is the continuity of knowledge of the fuel assemblies from the encapsulation facility to the repository, which requires containment and surveillance measures. Following the proposal of the Swedish Nuclear Fuel and Waste Management Company (SKB), spent fuel is encapsulated in copper canisters with a cast iron insert in an encapsulation facility, transported by ship approximately 300 nautical miles and then emplaced underground. These canisters will be marked with an engraved identification tag on the lid that includes the country of origin, serial number and a control digit. Ideally, this identifier is unique and cannot be falsified.

In a previous work, we presented coherent scanning interferometry (CSI) as a non-invasive optical measurement technique to identify the naturally occurring manufacturing artefacts of the engraving process at the bottom of the identification characters as unique fingerprint for canister authentication.

In this work, we introduce two alternative techniques for copper canister authentication, namely laser triangulation (LT) and direct feature comparison in microscope images. We will discuss their advantages and drawbacks with respect to CSI. Laser triangulation is a non-contact optical surface metrology technique that allows 3D reconstruction of surfaces based on the geometrical arrangement between a line laser, the target and a range camera. Both techniques, LT and microscope image processing, could be easily implemented as compact detection instruments for the field and allow fast data acquisition and results.

By comparing different copper samples with the same engraved identification tag for cross-sample analysis, we evaluate the performance of both techniques for authentication purposes. Our work underpins a potential pathway to nuclear safeguards of spent fuel containers and has implications for cross-disciplinary areas, such as general surface authentication or forensic analysis.

### INTRODUCTION

Various countries have aimed for long-term geological repositories to store spent fuel from nuclear reactors. The spent fuel elements will be encapsulated in copper canisters with a cast iron insert [1], transported by ship, lowered into the ground until a depth of about 500 metres and subsequently embedded in bentonite clay [2], in accordance with the proposal of the Swedish Society for Nuclear Fuel and Waste Management (SKB). The outer casing of the encapsulation canisters consists of a base plate, a cylindrical tube and a lid made entirely of copper and welded via Friction Stir Welding (FSW). Copper is selected due to its favourable material properties, such as corrosion resistance, heat transfer and load capacity. The final canisters are 4.835 m high, 1.050

m wide and will be equipped with an identification tag on the lid, realized through a Computer Numerical Control (CNC) system.

In the past we demonstrated that Coherent Scanning Interferometry (CSI), a technique based on white light interference, is capable of three dimensionally reconstructing the milling traces within this engraved identification tag and using them as unique fingerprint for canister authentication [3]. As an all-optical technique, it has the advantage of being non-invasive and by exploiting the interference signals of light, offering very high precision in depth measurements. Nevertheless, interferometric instruments require usually a controlled laboratory setting and several challenges have to be addressed for their application in an industrial surrounding.

First, even commercial CSI instruments need several minutes to collect data, which requires a vibration-free environment—something that is rarely available in an industrial setting. This may necessitate the introduction of active [4] or passive feedback mechanisms [5] to track and/or directly correct unavoidable displacement changes during the measurement process that increases system complexity and adds more potential sources of error by requiring additional electrical and optical components as well as a carefully timed acquisition process.

A final reading device also needs to work in a genuine industrial setting. It should be reliable and simple to use, ideally in the form of a mobile, compact reading system that requires minimal human intervention. It is a challenging task to automate each component and process in an interferometric microscope to meet this requirement.

Additionally, everything contaminating the surface and therefore changing its reflectivity (e.g. dust, oxidation and other reactions with chemical substances) or changing the illumination conditions (misalignment, variation in brightness) has an effect on optical authentication techniques, which constitutes an obvious drawback. Thus, a robust authentication scheme requires a technique capable of discriminating between measurements of the same and different surfaces in presence of these to a certain degree unavoidable effects.

In this work, we are evaluating two alternative optical approaches and comparing their performance in authenticating the copper string identifier. The first approach evaluates the performance of different feature recognition algorithms by directly comparing the 2D microscope images without surface reconstruction, taken by our CSI system. The second approach presents a Laser Triangulation (LT) system prototype, based on a similar principle as the Laser Mapping for Containment Verification (LMCV) [6] system for container welds, for identifying variations of the 3D surface of the identifier string engraved on the copper lid. Both methods would have the benefit of requiring a less complex setup layout than a full CSI system, making them easier to implement in the field.

## **SAMPLE DESCRIPTION**

The foreseen identifiers of the copper canisters will be composed of seven characters (**Figure 1**) using either the “Medium 10 DIN 1541” or the “KUHLMANN Groteskschrift” as font. As illustrated in **Figure 1**, each character has a height of  $10 \pm 1$  mm with an engraving width of  $1.5 \pm 0.3$  mm and depth of  $0.7 \pm 0.2$  mm.

For cross-sample analysis, we will look into six different test samples that mimic potential canister identifiers and where already investigated via CSI [3]. Each sample measures 140 mm in length and 40 mm in width. In order to prevent structural deformation over time, a thickness of 10 mm

was chosen. A CB Ferrari B13 3 Axis CNC machine engraved the characters utilizing the common Medium DIN 1541 font. **Figure 1** displays an example sample along with the string's corresponding dimensions.

The microscope image comparison will only consider a portion of the control digit limited by the field of view of the objective lens (indicated by the red square around part of the control digit in **Figure 1**), as opposed to the LT setup that record the entire string identifier for authentication.



**Figure 1. Example of engraved identifier on a copper sample. The measures of the characters are shown below.**

Repeated measurements on the same sample involved cleaning steps in between the measurements, remounting (misalignment) and/or slightly changing the illumination to simulate the conditions in a real world environment.

## **MICROSCOPE SYSTEM**

The first approach for copper canister authentication that we investigate in this work is based on a direct comparison of 2D microscope images taken of the control number milling traces. This approach has the unarguable advantages of a single shot technique, being fast, insensitive to vibrations, sufficiently easy to implement as a compact instrument and without the need for sophisticated surface reconstruction algorithms. We tested this approach using the setup built for coherent scanning interferometry [3] by blocking the interferometric path in the microscope objective lens to consider solely the image without interference signal. The final image was therefore formed by an infinity corrected Nikon CF IC EPI Plan TI objective with 2.5X magnification in conjunction with a 200 mm Nikon tube lens, leading to a field of view of 5.625 x 4.125 mm.

We analysed the microscope images with three common image comparison techniques, implemented in openCV [7] and defined our figures of merit based on the characteristics of the used technique:

- 1) Template matching and normalized cross-correlation coefficient.
- 2) Feature recognition based on the ORB algorithm and averaged normalized Hamming distances.
- 3) 2D registration and figure of merit based on difference statistics.

## MICROSCOPE RESULTS AND DISCUSSION

### Template matching

A basic method to compare two signals consists in the derivation of the normalized cross-correlation. Template matching can be understood as its two dimensional counterpart. It is a method for searching the location of a so-called template image (smaller part of an image) in the original image. The area where the template matches with the source image is identified by sliding the template pixel by pixel over the comparison image and calculating a metric, which indicates the quality of the match. For the microscope images, we used the normalised cross-correlation coefficient as metric, resulting in -1 in the case of completely uncorrelated image parts and giving 1 only for perfect correlation.

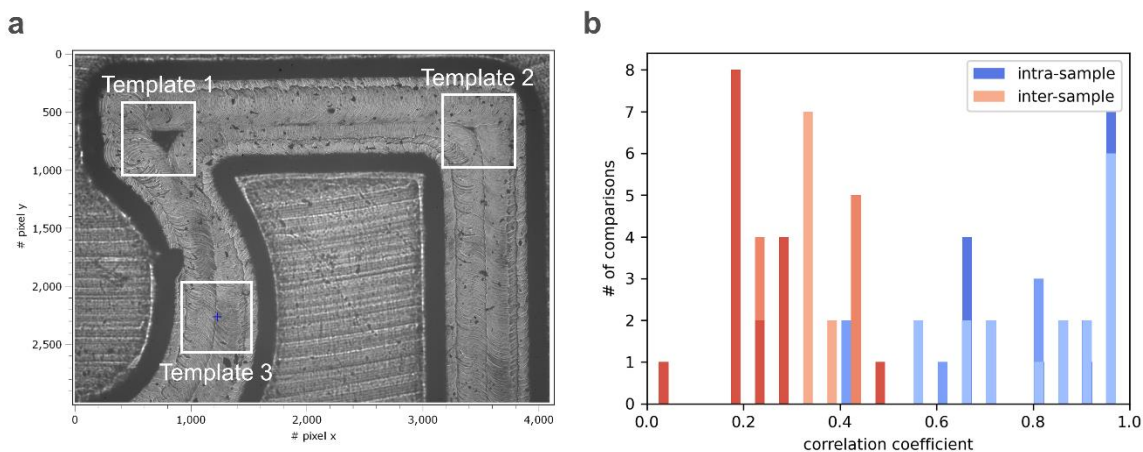


**Figure 2. a) Example templates of different parts b) Correlation coefficients of the different template choices.**

The resulting distributions strongly depend on the chosen template (**Figure 2 a**). As **Figure 2 b** shows, the correlation coefficient distributions quickly start overlapping. For an authentication task, this would result in false positive and negative results, rendering the method unreliable. A good template requires characteristic and unique image features that clearly distinguish the chosen surface part from other samples. Finding and defining a template with significantly unique image features in our particular case is difficult, since the milling traces of the characters show only slight variations between the different copper samples. Therefore, even non-matching samples exhibit areas which are similar enough to produce correlation coefficients almost as high as from data taken on the same sample, considering that slight alignment shifts, which change the shadowed areas and the presence of dust can lower the correlation coefficient even for matching samples.

### Feature recognition based on ORB algorithm

Oriented FAST and Rotated BRIEF (ORB) was developed by Ethan Rublee et al. in 2011 [8] at openCV labs, as an alternative to SIFT and SURF algorithms. In contrast to the latter, ORB is not patented and therefore free to use. The algorithm identifies and relates keypoints for image comparison. To analyse the microscope images, we chose the normalized Hamming distance as matching criterion, and calculated the average distance of the matching keypoints as figure of merit. Repeated measurements on the same samples showed a wide spread of values with overlapping distributions of inter- and intra-sample comparisons. Since a good keypoint should

be invariant to lighting conditions, angle, scale and background, the algorithms are programmed in such way that they select corresponding image features. Therefore, the algorithm is sensitive to high contrast edges and blob like image features. Being an advantage in regular feature detection applications, like object/motion tracking or face-matching, it constitutes a drawback in our application case, since every dust particle present on the sample embodies a perfect detection target and will be preferably selected as suitable keypoint. This leads to wrong matching keypoints assignments and renders the algorithm too error-prone for our case.

### 2D registration and difference statistics

In parametric image alignment, the problem consists of finding a transformation, which aligns two image profiles that can be entire images, sub-images or more complex tasks, like region tracking and motion estimation. The ECC image alignment algorithm implemented in OpenCV is based on a publication by Evangelidis et al. [9], where a similarity measure called Enhanced Correlation Coefficient (ECC) for estimating the parameters of the motion model is suggested. The alignment problem can be understood as mapping between the coordinate systems of two images. The first step consists of selecting a suitable model. Taking into account that we are using an aberration corrected objective lens with limited depth of field to produce a sharp image of the region of interest (ROI), we chose the Euclidean motion model for image comparison, based on translations and rotations, to map between two images. After image registration, the images were first masked to consider solely the values of the engraved character and subsequently the differences between the remaining areas as well as their distributions calculated.

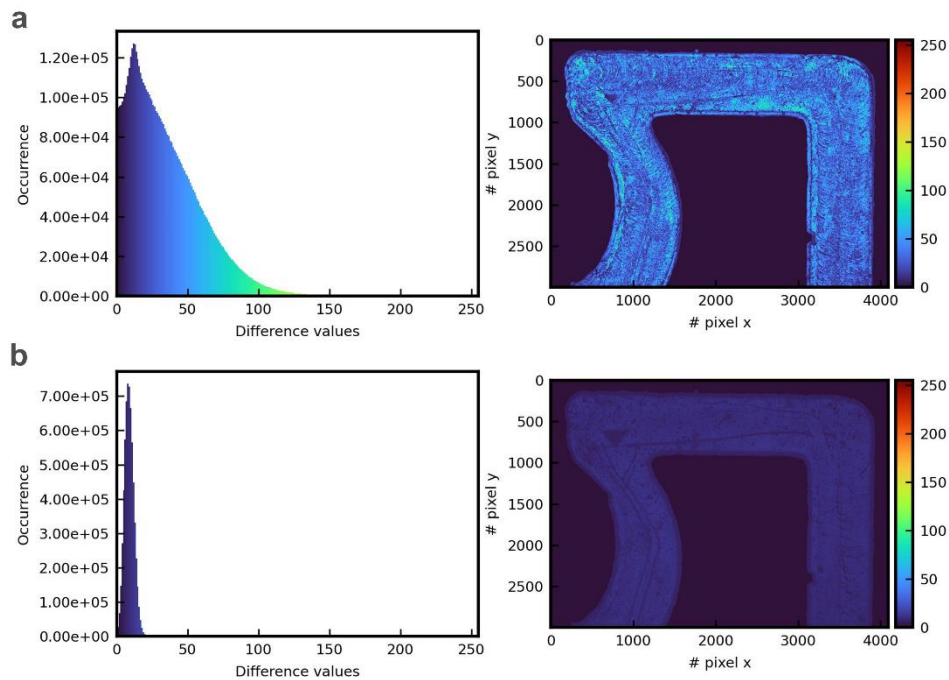


**Figure 3. a) Comparison of sample #4 with sample #7. b) Comparison of sample #4 with slightly changed illumination conditions.**

Analogous to the comparison of the three dimensional surface maps from CSI [3] and LT measurements, the intensity differences between registered images were evaluated based on their characteristic distributions (**Figure 3**) and a comparison parameter defined. The distributions of the above figure of merit for inter- and intra-sample measurements (**Figure 4**) are better

distinguishable with respect to template matching or feature recognition using the ORB algorithm. Nevertheless, one outlier is visible in the dataset, due to failure of the ECC algorithm for this particular dataset. The presence of dust particles and the use of cleaning procedures involving chemical agents (solvents) can influence the reflectivity from the surface and broaden the distribution of difference values. Combined with misalignment that significantly alters the distribution of shadowed areas, this can lead to failure of the ECC registration and generate outliers, leading to wrong negative results in an authentication procedure.

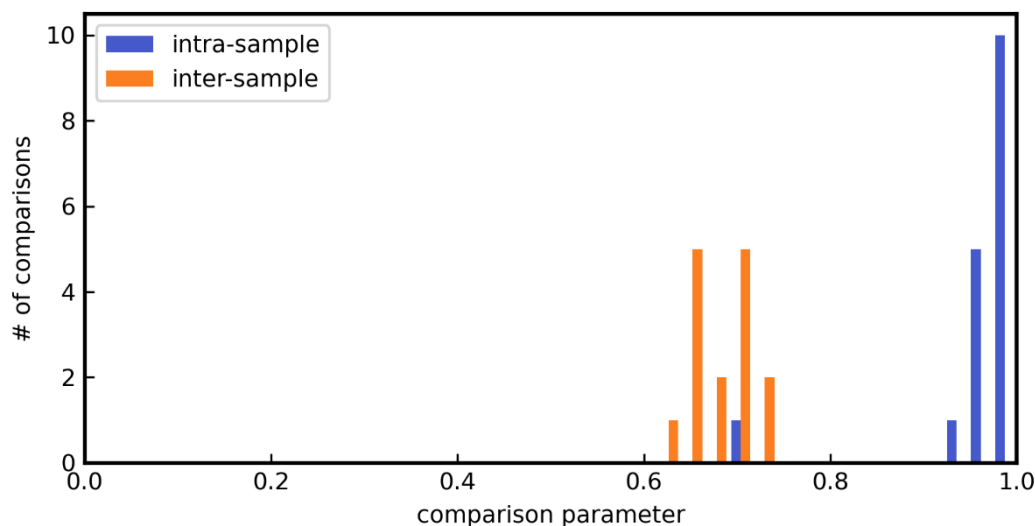


**Figure 4. Results of image registration and difference statistics.**

## LASER TRIANGULATION SYSTEM

Laser triangulation is a non-contact optical measurement technique that allows reconstructing the absolute distance and 3D shape of a target object [10]. The main optical components of our test system are a blue Z-laser Z20-XS20-HC-F-450-elp75 laser, with 450 nm wavelength, 20 mW output power and 75° aperture angle, which projects the laser line on the object to measure, and a SICK Ranger3 range camera placed at a certain angle from the laser source (**Figure 5**). The shorter wavelength was chosen to reduce speckle noise on the image sensor. The laser light intersecting the target surface is diffusely reflected towards the camera sensor. Part of the reflected laser light is imaged by a MeVis C-Mount lens with 35 mm focal length onto a detector array, in our case a complementary metal-oxide-semiconductor (CMOS) sensor [11], having a resolution of 2560 x 832 pixels with 6 μm pixel size and a scan rate of 2500 3D profiles in full format per sec.

The depth differences of the target object can be calculated via simple trigonometric relationships, knowing the triangulation angle ( $\alpha$ ), which is the angular offset between the laser source and the camera. As depicted in **Figure 5 a**, the distance to the target surface and the laser/camera configuration determines where on the camera sensor the laser light is detected. To measure the laser line centre projected on the detector, peak finding algorithms are employed [12], producing a 3D reconstruction of the target surface contour. A PIL-741 High-Precision XY linear translation stage shifted camera and laser components horizontally during the acquisition process in order to reconstruct the whole characters string of the copper samples. The measurement range depends on the triangulation angle of the system. A smaller triangulation angle corresponds to an increased measurement range but also to a lower resolution of the depth measurements. The in-house manufactured support arm has the predisposition to fix the camera at an angle of 30°, 45° or 60°

with respect to the horizontal line. The laser, instead, can be mounted at an angle of  $0^\circ$ ,  $30^\circ$ ,  $45^\circ$  or  $60^\circ$  with respect to the vertical line. Based on the results of the experimental tests, the classical triangulation configuration with the laser source positioned at  $0^\circ$  and the camera tilted at  $45^\circ$  offered the optimum compromise between height resolution and surface occlusion.

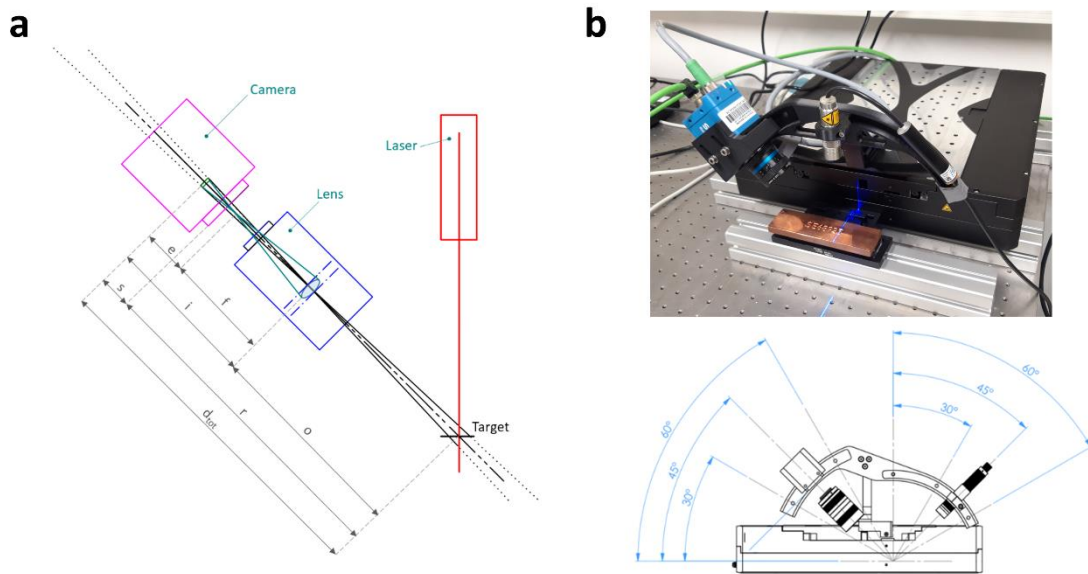


**Figure 5. a) Optical scheme of standard triangulation system. b) Implemented triangulation setup prototype with configuration possibilities.**

To ensure that the entire height of the object is in focus, a Scheimpflug configuration (6.0 degrees angle) was used by tilting the camera sensor plane with respect to the lens plane [13]. For the control of the instrument, an in-house C++ application was developed, allowing easy configuration of scan and hardware parameters and fully automated data acquisition using self-built libraries for translation stage and range camera. The software saves the data directly in 3D point cloud format with the help of a lookup table that maps the 2D pixel coordinates of the laser line detected on the camera sensor into 3D range values, calculated based on the used setup geometry. The final surface topographies were further processed employing the Python extension Open3D.

## TRIANGULATION RESULTS AND DISCUSSION

The reconstructed surface point clouds of all measured samples were aligned via point cloud registration [15], [16] and their point-to-plane distances calculated using the same routine as for the CSI measurements (for details, please refer to Neutzner et al. [3]). **Figure 6** shows the exemplary distance distribution (**Figure 6 a**) and map (**Figure 6 c**) for intra-sample and inter-sample measurements between sample #5 and #6. Although less pronounced than in the case of the CSI measurements, the detectable deviations in surface structure appear in the distributions of inter-sample measurements and a similar trend can be observed. Only 64% ( $\pm 2.1\%$ ) of the distributions for inter-sample measurements fall within an interval up to  $5 \mu\text{m}$ , compared to 90.2% ( $\pm 4.5\%$ ) of the distance distributions for intra-sample data.

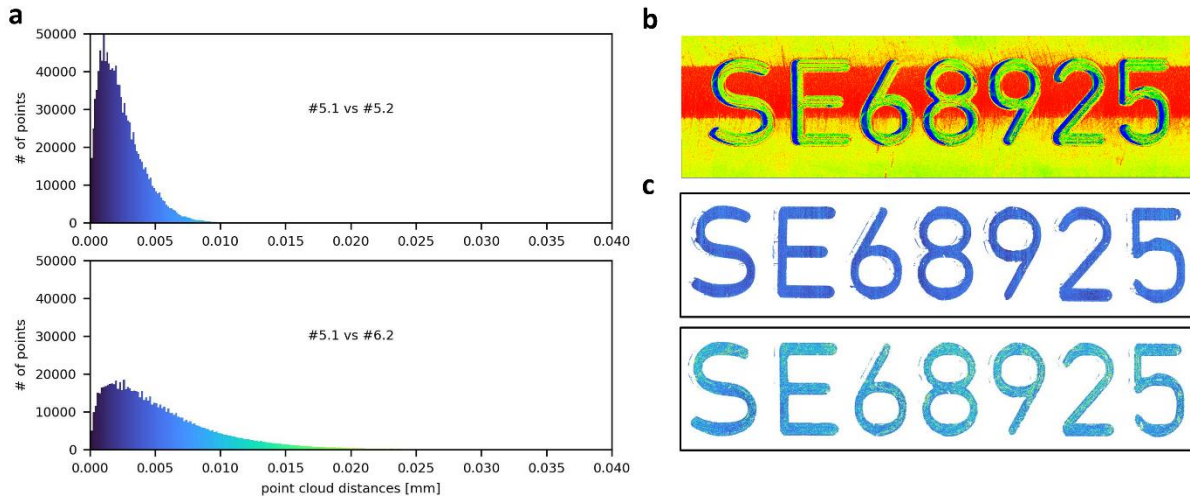


**Figure 6. a) Distance distributions of sample #5 and #6. b) Raw point cloud after the scan. c) Distance maps between sample #5 and #6.**

In analogy to the evaluation of the CSI measurements, we define a comparison parameter ( $cp$ ) for the LT dataset, considering the above characteristic distance distributions present during the data analysis.

$$cp = \frac{\int_0^5 n(x) dx}{\int_0^{40} n(x) dx}$$

Here,  $n(x)$  describes the occurrence of calculated point-to-plane distances of correlated points over the distance interval  $x$ , within a total range from 0 to 40  $\mu\text{m}$ . The results of all sample comparisons are shown in **Figure 7 a**.

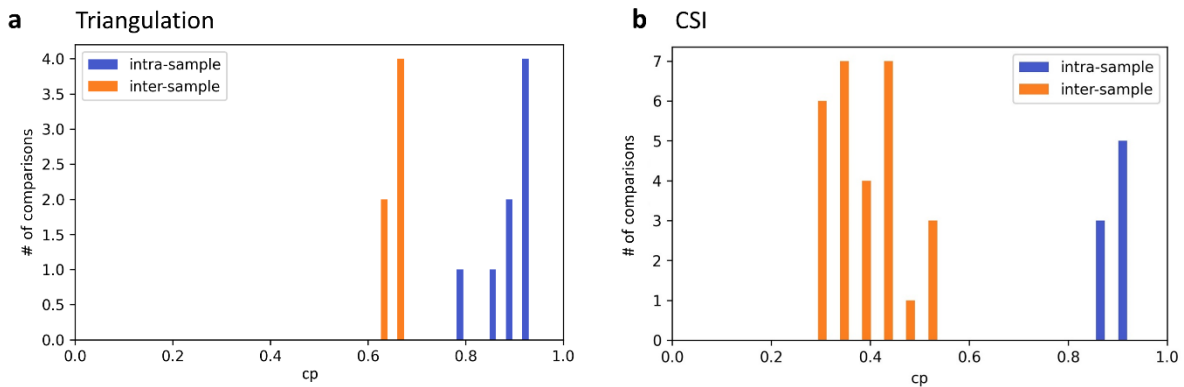


**Figure 7. a) Distribution of comparison parameter for the LT measurements. b) Distribution of comparison parameter for the CSI measurements (adapted from [3]).**

The distributions for the samples we investigated do not overlap. However, they also do not exhibit the same grade of separation between inter- and intra-sample measurements, as it has been demonstrated with surface reconstructions acquired with the CSI technique (**Figure 7 b**). The depth resolution of the LT system is limited by its laser linewidth ( $\sim 55 \mu\text{m}$ ), and therefore it is impossible to resolve traces caused by the rotational movements of the CNC milling head, present in the CSI surface topographies, which lie in the range of tens of nm to few  $\mu\text{m}$ . Only bigger

scratches in the order of several to tens of  $\mu\text{m}$ , caused by the lateral movements of the tool, can be resolved. Therefore, reconstructed surfaces exhibit intrinsically higher similarity between different tag copies, since their fine surface details are buried in noise.

## **CONCLUSIONS**

None of our investigated 2D image algorithms was able to assign all investigated copper samples correctly. ECC registration with subsequent analysis of the difference statistics proved to be the best performing technique for authentication purposes, resulting in separated distributions of the selected figure of merit and exhibiting only one false negative result. Taking into account values from all pixels of the investigated surface image, the algorithm appears to be more robust with respect to dirt and dust particles but turns out to be highly sensitive to changes in reflectivity and fails in presence of a combination of different environmental factors. One factor that would influence the accuracy of using a simple microscope for canister authentication is aging of the copper surface. Although it is foreseen that the period between referencing and authentication of the canisters will be of few months and strong oxidation is not expected to happen, even slight changes in surface reflectivity alter the results of a 2D comparison as we observed. Additionally, these changes might not happen uniformly, depending on the storage and transport conditions of the cylinders. Considering all the factors that need to be controlled for a proper 2D image comparison reveals the advantages of the investigated LT 3D technique that allows to measure the whole string identifier, does not require such strict controls of environmental conditions and demonstrated to assign each sample correctly. By processing the 2D images to extract surface information and performing the registration on the processed 3D dataset, misalignment and slight changes in surface reflectivity do not affect the outcome. Solely the presence of a substantial amount of dust or dirt can potentially influence the LT and CSI techniques by scattering the laser beam and reducing the intensity of the reflected interference signal, respectively. In a controlled environment, CSI is the best performing technique showing the highest discriminative capacity due to its superior depth resolution. Nevertheless, both 3D techniques would need further tests in a real world environment to evaluate their authentication performances and applicability in the field.

## REFERENCES

1. Hedman, T., Nyström, A., & Thegerström, C., *Swedish containers for disposal of spent nuclear fuel and radioactive waste*, Comptes Rendus Physique, Vol. 3(7-8), pp. 903-913 (2002).
2. Hildingsson, L., Andersson, C., & Fagerholm, R., *Safeguards aspects regarding a geological repository in Sweden*, (No. IAEA-CN--220), (2015).
3. Neutzner, S., Fassi, A., & Boström, G., *Coherent scanning interferometry for copper canister authentication and applied forensics*, INMM Annual Meeting Proceedings, (2023).
4. Martin, H., Wang, K., & Jiang, X., *Vibration compensating beam scanning interferometer for surface measurement*, Applied optics, Vol. 47(7), pp. 888-893, (2008).
5. Tereschenko, S., Lehmann, P., Gollor, P., & Kuehnhold, P., *Vibration compensated high-resolution scanning white-light Linnik-interferometer*, Optical Measurement Systems for Industrial Inspection X, Vol. 10329, pp. 992-1002, SPIE, (2017).
6. Taddei, P., Boström, G., Puig, D., Kravtchenko, V., & Sequeira, V., *Container weld identification using portable laser scanners*, Journal of Electronic Imaging, 24(2), 023005-023005, (2015).
7. Bradski, G., *The openCV library*, Dr. Dobb's Journal: Software Tools for the Professional Programmer, Vol. 25(11), pp. 120-123, (2000).
8. Rublee, E., Rabaud, V., Konolige, K., & Bradski, G. (2011, November). ORB: An efficient alternative to SIFT or SURF. In 2011 International conference on computer vision (pp. 2564-2571). IEEE.
9. Evangelidis, G. D., & Psarakis, E. Z. (2008). Parametric image alignment using enhanced correlation coefficient maximization. IEEE transactions on pattern analysis and machine intelligence, 30(10), 1858-1865.
10. Ji, Z. and Leu, M.C., *Design of optical triangulation devices*, Opt. Laser Technol., Vol. 21, pp. 339–341 (1989).
11. Liebe, C.C. and Coste, K., *Distance Measurement Utilizing Image-Based Triangulation*, IEEE Sens. J., Vol. 13, pp. 234–244 (2013).
12. Kienle, P., Nallar, E., Köhler, M.H., Jakobi, M. and Koch, A.W., *Analysis of sub-pixel laser spot detection in laser triangulation systems*, Proceedings of the SPIE, Vol. 11056, pp. 933–943 (2011).
13. Li, J., Guo, Y., Zhu, J., Lin, X., *Large depth-of-view portable three-dimensional laser scanner and its segmental calibration for robot vision*, Optics and Lasers in Engineering, Vol. 45(11), pp. 1077–1087 (2007).
14. Zhou, Q. Y., Park, J., & Koltun, V., *Open3D: A modern library for 3D data processing*. arXiv preprint arXiv:1801.09847, (2018).
15. Choi, S., Zhou, Q. Y., & Koltun, V., *Robust reconstruction of indoor scenes*, Proceedings of the IEEE Conference on Computer Vision and Pattern Recognition, pp. 5556-5565, (2015).
16. Rusinkiewicz, S., & Levoy, M., *Efficient variants of the ICP algorithm*, Proceedings third international conference on 3-D digital imaging and modelling, pp. 145-152, IEEE, (2001).